



King Saud University
Arabian Journal of Chemistry

www.ksu.edu.sa
www.sciencedirect.com



ORIGINAL ARTICLE

Efficient synthesis of new azo-sulfonamide derivatives and investigation of their molecular docking and cytotoxicity results



Nosrat O. Mahmoodi ^{a,*}, Ali Ahmadi ^a, Hadiseh Yazdani Nyaki ^a,
Hossein Taherpour Nahzomi ^b, Esmael Panahi Kokhdan ^c

^a Department of Organic Chemistry, Faculty of Science, University of Guilan, Rasht, Iran

^b Department of Chemistry, Payame Noor University, Tehran, Iran

^c Medicinal Plants Research Center, Yasuj University of Medical Sciences, Yasuj, Iran

Received 2 July 2022; accepted 21 October 2022

Available online 29 October 2022

KEYWORDS

Azo sulfonamide;
Antioxidant;
Cytotoxic;
Molecular docking;
MTT assay;
Molecular dynamic

Abstract The present study focused on the synthesis, introduction and investigation of the biological effects of sulfonamide-derived products as new azo-sulfonamides (samples 1–6). In this transformation, the amine sulfonamide is first converted to the corresponding diazonium salt, which is then attacked by a nucleophilic carbon of the aromatic ring in the playing medium. All products were obtained with reasonable yields and high purity. The structure of synthesized derivatives was determined using various analytical tools including FT-IR, ¹H NMR, ¹³C NMR and XRD spectroscopy, and the synthesized products were purified and identified. Biological properties of newly synthesized azo-compounds similar to SSZAD were also investigated. These compounds were tested in terms of biological effectiveness. The results of biochemical assays show that: the products have significant biological properties. MTT toxicity of compounds in breast cancer cells (MCF-7) for compounds 1–6 according to IC₅₀ compare to Vinblastine is Vin > 5 > 4 > 6 > 2 > 3 > 1. The biochemical results obtained were analyzed by molecular docking interaction studies and showed strong hydrogen bonding with the target receptor. The docking calculation has been invoked to reveal the type of interactions that synthesized compounds can establish with the residues forming the active sites of the target proteins. 1FDW the three higher scores molecules appears to be (6 > 1 > 2), 3FC2 (the three highest binding affinities are in the order of 1 > 3 > 6), and 5GWK (three highest binding affinities are 1 > 3 > 6). The results indicate the effective interaction

* Corresponding author.

E-mail addresses: mahmoodi@guilan.ac.ir (N.O. Mahmoodi), h_taherpour@pnu.ac.ir (H. Taherpour Nahzomi), esmaeel_panahi@yahoo.com (E. Panahi Kokhdan).

Peer review under responsibility of King Saud University.



<https://doi.org/10.1016/j.arabjc.2022.104383>

1878-5352 © 2022 The Author(s). Published by Elsevier B.V. on behalf of King Saud University.

This is an open access article under the CC BY-NC-ND license (<http://creativecommons.org/licenses/by-nc-nd/4.0/>).

of all products with the targets. The molecular dynamics simulation has been invoked to study the presence of a stable system of the interacting protein–ligand.

© 2022 The Author(s). Published by Elsevier B.V. on behalf of King Saud University. This is an open access article under the CC BY-NC-ND license (<http://creativecommons.org/licenses/by-nc-nd/4.0/>).

1. Introduction

Cancer is one of the leading causes of death worldwide, and breast cancer is one of the most common cancers in women that originates in breast tissue cells (Burden et al., 2018; Elsellami, 2008; Sharma et al., 2010; Smith and Mallath, 2019; Sung et al., 2021). Female sex hormones and estrogen can stimulate the development, proliferation, migration, and survival of target cells and the development of secondary sexual characteristics (Agre et al., 2021; Lina, 2021; Shaikh et al., 2021). Estrogen acts by binding to estrogen receptors (ER), which are members of the nuclear receptor transcription factor superfamily that highly conserved DNA and ligand-binding domains characterize. Nuclear receptors play an essential role in gene expression. This gene mutation leads to the production of an abnormal estrogen receptor, also known as ER+, which results in breast cancer in women (Bakadia et al., 2022; Camarillo et al., 2021; Mane et al., 2021; Wellings and Jensen, 1973).

Azo molecules have a characteristic azo bond (-N=N-) and are considered interesting roles in organic chemistry (Crespi et al., 2019). Since the last century, these color compounds have been widely used as dyes in various industries in applications such as printing, food, paper, cosmetics, laser, electronics, optics, material science, etc. The discovery of Prontosil, an antibacterial drug, thrust azo compounds into the attention of the field of medicinal chemistry (Cockerham et al., 2022). Azo biologically active molecules play a vital role in medicine and pharmacology, in other words, all Schiff base derivatives are therapeutic (Pervaiz et al., 2021). They have a wide range of industrial and pharmaceutical applications and are specific biologically particular, such as antibacterial (Gaffer, 2019), antifungal (Węglarz-Tomczak and Górecki, 2012) anti-inflammatory (Keshavayya, 2019), antimicrobial (Gaffer, 2019), anti-malarial, anti-cancer (Ali et al., 2018), anti-tuberculosis (Ravi et al., 2020), and anti-viral.

Sulfasalazine (SSZ) compounds have many metabolic properties, including antibacterial, anti-malarial, anti-fungal, antioxidant, as well as anti-viral and anti-cancer agents (Choudhary et al., 2015; Gomberg and Bachmann, 1924; Gordon and Gregory, 2022; Hari and Koenig, 2013; Nemati and Elhampour, 2012; Parekh, 2010; Peters and Freeman, 1991).

Due to the anti-cancer pharmacopeia properties of azo and SSZ compounds in order to continue the interest of our research group in the synthesis of new azo-drug compounds, and to investigate their XRD, molecular docking, and cytotoxicity results (Ansari et al., 2022; Gilani et al., 2008; Mahmoodi et al., 2017, 2013; Malaekhepoor et al., 2020; Nadamani et al., 2019; Nyaki and Mahmoodi, 2021; Sheykhi-Estakhjani et al., 2020) here, synthesis of several new SSZAD was reported. These new compounds were evaluated for their antioxidant and anti-cancer properties.

2. Results and discussion

2.1. Chemistry section

Azo products are usually produced in two stages. The first step of the de-annotation reaction: with the primary type of aromatic amine of sulfonamides, an aqueous mineral acid such as HCl and sodium nitrite (NaNO_2) is mixed as a source of in-situ nitrosonium ion ($\text{N}^+ = \text{O}$) construction in an ice bath to produce diazonium salt. This salt is unstable at r. t., since diazonium salts gradually decompose even at low temperatures, so it is produced at 5° C (Kumar et al., 2010; Sharma et al., 2020). The mate must have active aromatic rings or active nucleophilic groups to participate in the electrophilic substitution reaction and bind to the diazonium salt Fig. 1 (Khan et al., 2021). The present study is to investigate the production and stability of diazonium salts using cellulose sulfuric acid as catalyst (Gaffer et al., 2017; Lee et al., 1988) and its purpose is to perform a coupling reaction to produce azo dyes under the solvent-free conditions. Cellulose sulfuric acid (CSA) as a solid acid has advantages such as biodegradability, cost-effectiveness, recyclability, and compatibility with green chemical ovens (Ganewatta et al., 2019).

By grinding sulfonamides and CSA with a few drops of water in a mortar, a homogeneous mixture was obtained. NaNO_2 was then added to the resulting mixture and gently ground for 2–3 min. The reaction mixture was reacted with the coupling agent for 10–20 min and the structure of the products was confirmed by FT-IR, ^1H NMR, and ^{13}C NMR spectra, shown in Fig. 2 and Table 1.

In the FT-IR spectrum, the sharp peaks at $\sim 1140\text{ cm}^{-1}$ and $\sim 1345\text{ cm}^{-1}$ correspond SO_2 . The average peaks in $1435\text{--}1480\text{ cm}^{-1}$ correspond to $\text{N}=\text{N}$. Existence of a broad band in $\sim 3400\text{ cm}^{-1}$ corresponds to $\text{O}-\text{H}$. Medium twin band at $2700\text{--}2850\text{ cm}^{-1}$ corresponding to H with carbon $\text{C}=\text{O}$ aldehyde (products 5 and 6), $\text{N}-\text{H}$ bending tape in R_2-NH $1550\text{--}1650\text{ cm}^{-1}$, $\text{C}-\text{H}$ symmetric tensile tape in CH_3 - $\sim 1380\text{ cm}^{-1}$ (product 4), Peaks in the range of $2860\text{--}3000\text{ cm}^{-1}$ related to $\text{C}-\text{H}$ aliphatic saturation. Wide and weak peaks in $3000\text{--}3100\text{ cm}^{-1}$ related to aromatic $\text{C}-\text{H}$, $\text{C}=\text{O}$ aldehyde stretching band in $1645\text{--}1765\text{ cm}^{-1}$ (products 5 and 6). Medium or strong peaks in $1630\text{--}1740\text{ cm}^{-1}$ are

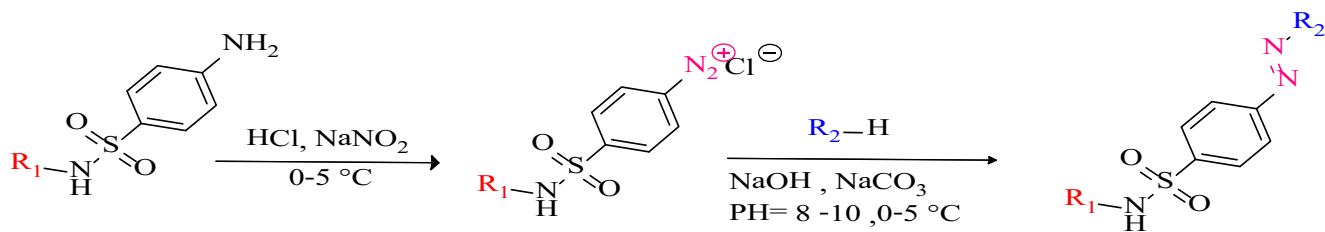
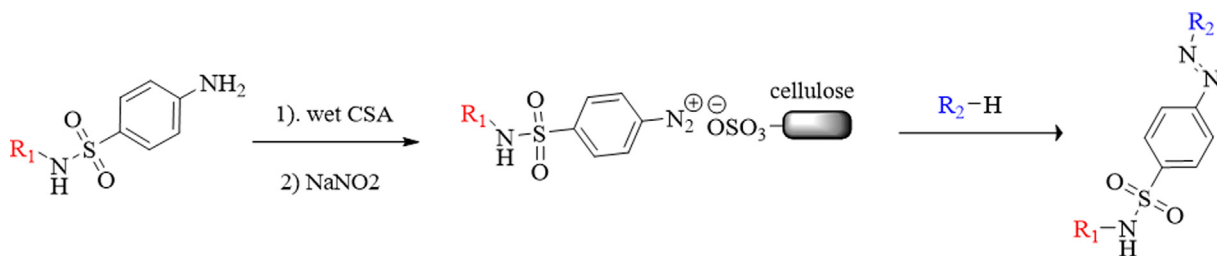


Fig. 1 Synthesis of azo-sulfonamide derivatives by azotation.



	1	2	3	4	5	6
R_1						
R_2						

Fig. 2 Synthesis of new azo-sulfonamides in the presence of CSA.

Table 1 New azo-sulfonamide derivatives synthesized using cellulosic sulfuric acid at room temperature.

Entry	Color	M.P (°C)	Efficiency (%)	Compounds
1		287 °C	81 %	
2		291 °C	83 %	
3		207 °C	64 %	
4		205 °C	74 %	
5		225 °C	87 %	
6		213 °C	79 %	

related to C=O amide and confirmed the structure of the desired products.

^1H NMR (MHz400) spectra of products were recorded in DMSO d_6 solvent. A singlet peak in the range of 2.20–2.60 ppm, confirms the presence of H-methyl of 3-methylisoxazol (products 3 and 6). Aromatic protons appeared in the expected range at 7.00–7.68 ppm, for products 1,2,3 and 4.

The O—H signal is appeared in the range of 15.01–15.90 ppm and confirms the presence of beta-naphthol in the product structure. In products 1 and 3, hydrogen bonds are formed between azo N bonds and O—H hydrogen bonds of beta naphthol and appear in the range 11.17–11.50 ppm. The C—H of thiazole ring appeared in product 4 in the range of 6.80–6.90 ppm and confirms the structure of the products. In the ^{13}C NMR spectra (100 MHz), aromatic carbon signals appeared at appropriate 117.00–146.30 ppm.

2.2. Investigation of X-ray diffraction (XRD) spectrum for the synthesized derivatives (4, 5)

The results of X-ray diffraction on the powder samples (4 and 5) were considered. The X-ray diffraction pattern of 4 is considered by the presence of four peaks at $2\theta = 13^\circ, 20^\circ, 23^\circ$ and 45° and for 5 the X-ray diffraction pattern is considered by the presence of seven peaks at $2\theta = 6^\circ, 9^\circ, 14^\circ, 20^\circ, 22^\circ, 26^\circ$ and 45° . Major peaks for both compounds appeared in the range of $2\theta = 10^\circ$ – 30° , indicating the relative similarity of the two compounds. XRD is a key technique for pharmaceutical analysis. It plays the main role in all the stages of development, testing and production of drugs. An important part of analytical research and development is quality control of active ingredients, excipients, and final products (Chauhan and Kaith, 2012, 2011). XRD study analyses the peak width along with lattice strain and lattice constants due to dislocation and particles size (Cullity, 1978; Mote et al., 2012). Particles size of the pure azo-sulfonamide are calculated using Scherer's Equation.

Here, D is the Particles size, βD is full width at half maxima, λ is the wavelength of $\text{CuK}\alpha$ radiation (1.54 Å) and 2θ is the Bragg peak position. Bragg peak broadening is the composition of both the effects i.e. instrumental as well as sample

dependent. The instrumental peak width was corrected according to each diffraction peak of azo-sulfonamide material using the following relation:

$$D = \frac{K\lambda}{\beta \cos\phi}$$

From the calculations the Particles size, the estimated value of Particles size for samples of azo-sulfonamide (4) and (5), respectively is 12.75 Å and 13.95 Å shown in Fig. 3.

3. Molecular docking study

To study and investigate the efficiency of the synthesized molecules as anticancer drugs the docking simulations in active sites of three target proteins of Human 17-Beta-Hydroxy Steroid Dehydrogenase (PDB ID: 1FDW), a member of the short chain dehydrogenase reductase (SDR) family, is responsible for the synthesis of 17beta-estradiol, the biologically active estrogen involved in the genesis and development of human breast cancers (<https://doi.org/10.2210/pdb1fdw/pdb>).

Human Serine/Threonine-Protein Kinase Receptor, (PDB ID: 3FC2) that performs several important functions throughout M phase of the cell cycle, including the regulation of centrosome maturation and spindle assembly, the removal of cohesins from chromosome arms, the inactivation of anaphase-promoting complex/cyclosome (APC/C) inhibitors, and the regulation of mitotic exit and cytokinesis (<https://doi.org/10.2210/pdb3fc2/pdb>). Human Topoisomerase II alpha (5GWK) were performed using Schrodinger program package (David et al., 2018). The ligands 1–6 structures have been located using the Gaussian 03 suite of programs Fig. 4 (Frisch et al., 2004). To perform the calculations the B3LYP model chemistry (Becke, 1993; Lee et al., 1988; Stephens et al., 1994; Vosko et al., 1980) in combination with the basis sets, 6-31G(d,p) (Blaudeau et al., 1997; Boys and Bernardi, 1970; Ditchfield et al., 1971; Francl et al., 1982; Hariharan and Pople, 1974; Hehre et al., 1972; Krishnan et al., 1980; McLean and Chandler, 1980; Rassolov et al., 1998; Stephens et al., 1994) for C, H, O, and N atoms and 6-311G(d,p) (Binning and Curtiss, 1990; Hariharan and Pople, 1973) for S atom were used (Kenchegowda et al., 2022). The 2D ligand-receptor interaction diagrams of the

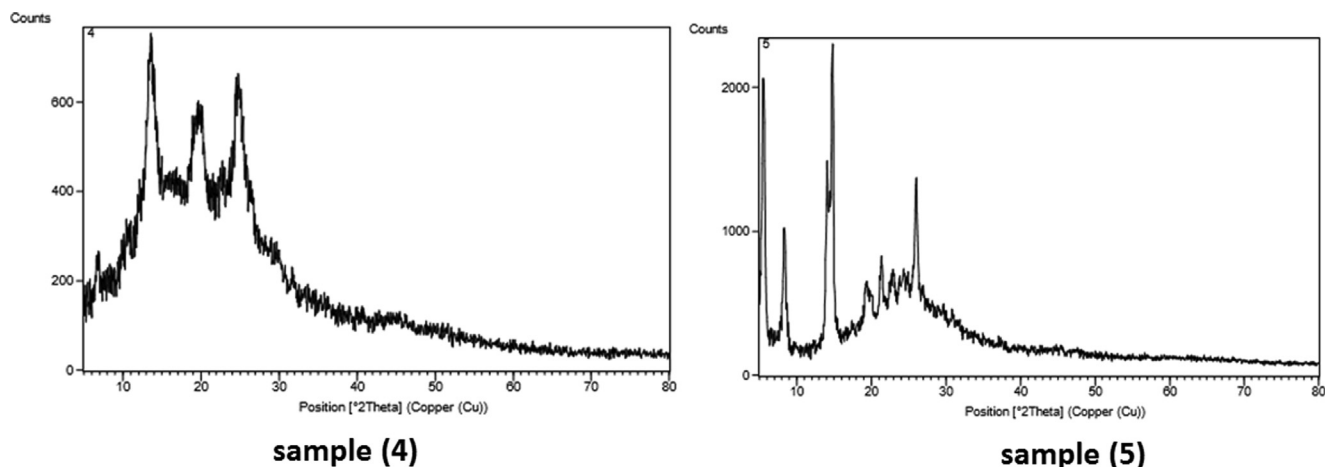


Fig. 3 X-ray diffraction pattern of samples (4, 5).

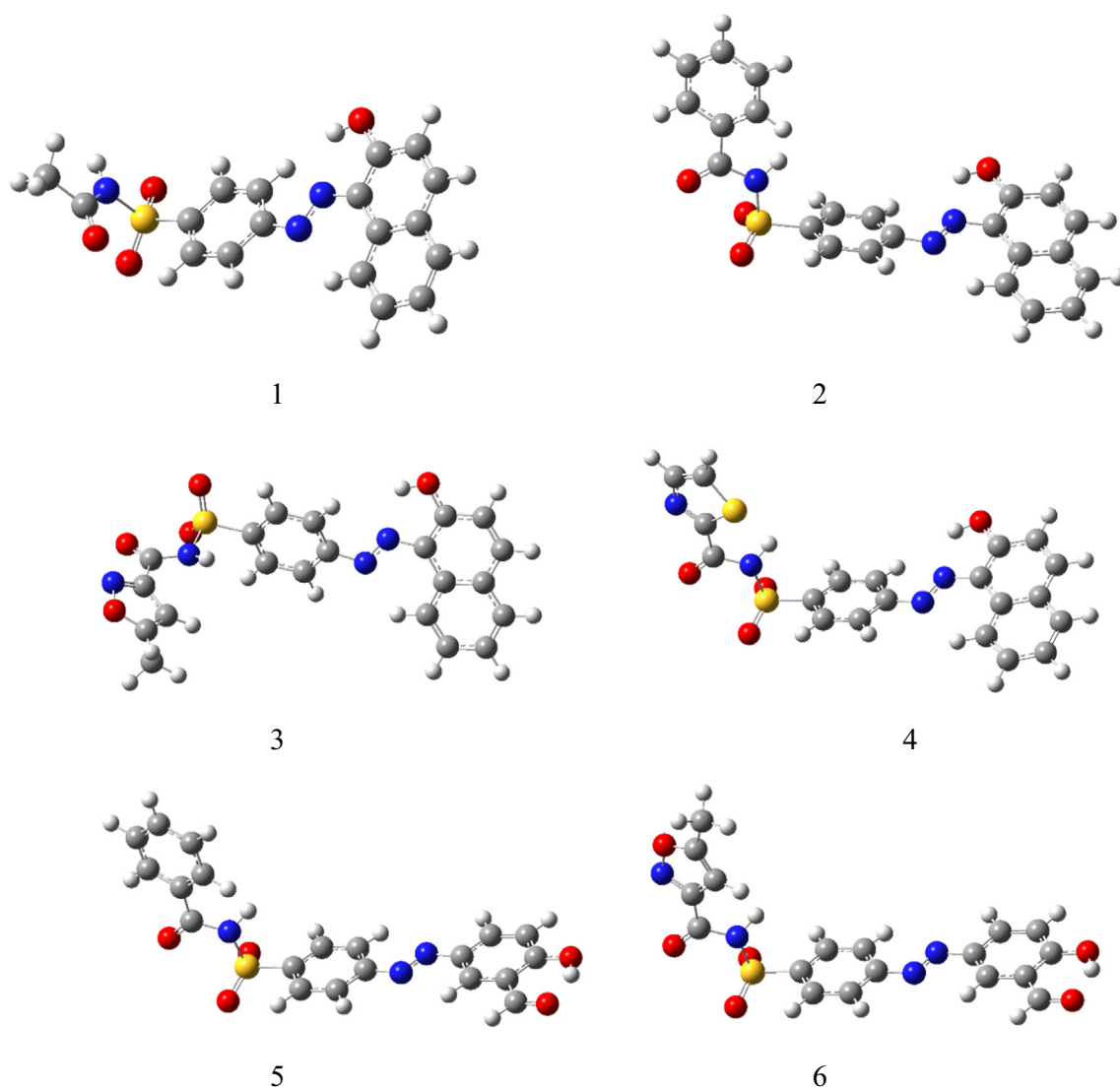


Fig. 4 The optimized structures were obtained at the B3LYP/6-31 + G(d,p)/ 6-311 + G(d,p) level of theory.

located structures with the targets and the 3D binding models of the compounds that have a high score to the mentioned receptors are displayed in [Figs. 5-7](#). Additional information on other compounds can be found in [Supporting Information](#). Furthermore, the relevant calculated binding affinity (Glide scores) have been collected in [Table 2](#).

3.1. Human 17-Beta-Hydroxy Steroid Dehydrogenase (PDB ID: 1FDW)

According to the docking results the order of binding energy of the three higher scores molecules appears to be $6 > 1 > 2$, respectively. In the case of 6, the nitrogen atom of the isoxazole ring behaves as an H-bond acceptor from the hydroxyl group of Tyr-218 residue by the distance of 2.47 Å, and the binding energy of the amount $-7.36 \text{ Kcal.mol}^{-1}$. From the 2D ligand-protein interaction diagram it is realized that the polar isoxazole ring fits very well in the pocket created by residues such as Leu-96, Tyr-218, Leu-219, Gln-221, Ser-222, and Lys-223. Structure 1 is posed in a different orientation relative

to 6, thereby getting the advantage of direct interaction with two surrounded residues. As the H-bond acceptor (HBA) between the phenolic group attached to the naphthalene moiety and Gln-221 on one side as well as the H-bond donor (HBD) type between amidic hydrogen and Glu-282. Although the present naphthalene group is unable to fit as well as the isoxazole ring present in 6 in the previously mentioned pocket but the presence of these two effective H-bonding interactions provides considerable stability, which ultimately leads to its high score. There is some extent of similarity when the 2D interaction diagrams of 1 and 2 are compared, but it is immediately apparent that lacking of the second observed interaction for 1 (between amidic hydrogen and Glu-282) in 2 leads to the less binding energy.

3.2. Human Serine/Threonine-Protein Kinase Receptor, (PDB ID: 3FC2)

Interestingly all structures display high Grid Scores and the three highest binding affinities are in the order of

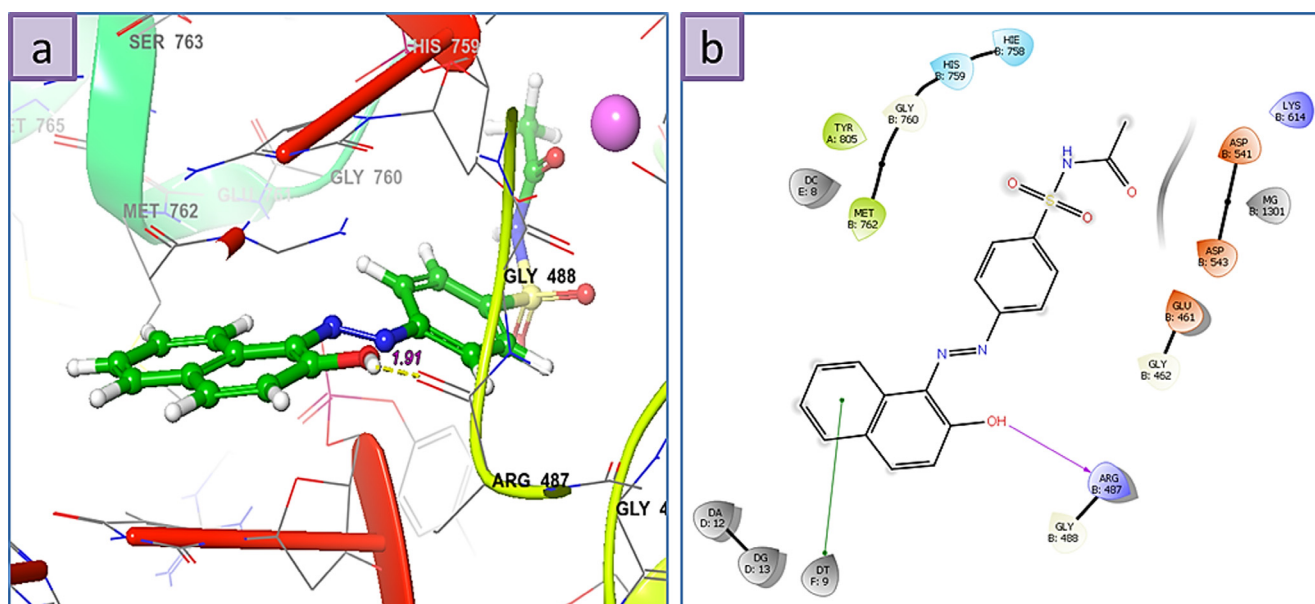


Fig. 7 a) 3D the binding mode of ligands with Human Topoisomerase II alpha (5GWK), b) 2D ligand-receptor interaction with 5GWK enzyme.

Table 2 Docking scores of the synthesized molecules (Kcal.mol^{-1}).

Ligand	Score		
	1FDW	3FC2	5GWK
1	-7.21	-8.04	-9.18
2	-6.04	-7.83	-7.68
3	-5.52	-7.54	-8.64
4	-5.72	-7.58	-7.84
5	-5.78	-7.23	-7.75
6	-7.36	-7.35	-8.17

group while at a place farther on the ligand the phenolic hydroxyl group takes part as HBD toward the Asp-541, an interaction not observed for any of the other present ligands.

3.3. Human Topoisomerase II alpha (5GWK)

Interestingly all structures show high Grid Scores and the three highest binding affinities are 1 > 3 > 6, respectively. The 3D ligand-protein interaction indicates appropriate and convenient stacking of ligands between the ruptured nucleotides forming a stable complex with the ability of inhibitory reattachment of the chains. The interchelating section of 1, 2, and 4 structures are mainly due to two rings naphthalene part and that of 3, 5, and 6 is benzene or hetero aromatic ring of amide part. Molecule 1 represents an H-bond interaction as HBD to the Arg-487 residue while the naphthalene ring establishes a stabilizing pi-pi stacking with deoxythymidine nucleotide (DT F:9). Molecule 2 shows pi-pi stacking of naphthalene moiety with DG D:13, middle benzene with DT F:9, and pi-cationic interaction between the benzene ring attached to amidic carbonyl group with the Arg-804. Molecule 3 shows pi-pi stacking of hetero aromatic ring with DA D:12 as well as

HBD from N-H to DT F:9. Molecule 4 shows pi-pi stacking of naphthalene moiety with DG D:13 and an H-bond interaction as HBD to the Arg-487 residue. Molecule 5 displays pi-pi interactions between the benzene ring attached to the amidic carbonyl group with DA D:12 and DG D:13 nucleotides, respectively. Furthermore, the oxygen atom of the carbonyl group accepts an H-bond from DC D:11. Finally, the isoxazole ring of 6 establishes a pi-pi stabilizing interaction with DT F:9 and at the same time, this nucleotide behaves as HBA from the N-H group while at a place farther on the ligand the phenolic hydroxyl group takes part as HBD toward the Asp-541, an interaction not observed for any of the other present ligands.

4. Molecular dynamics

4.1. Computational methods

System Preparation. The crystal structure of Human Serine/Threonine-Protein Kinase Receptor (PDB ID: 3FC2) was used as the initial structure and hydrogen atoms of the protein residues were added using LeAP (Song et al., 2019). The ligands were placed in the position determined by the previous docking process. The system was then soaked in a cubic box of 15,166 TIP3P water molecules extending to at least 15 Å from the protein atoms. The ff99SB force field (Ganjali et al., 2008) was used to describe the protein, together with General Amber Force Field (GAFF) (Wang et al., 2004) parameters for ligand.

MD Simulation. The simulation was carried out using the AmberTools 19 Molecular Dynamics package (Song et al., 2019). The system, prepared as described above, was first subjected to 1000 steps of steepest descent and 1000 steps of conjugate gradient minimization. The system was then heated to the target temperature of 300 K for a period of 20 ps under constant volume periodic boundary conditions (NVT). Subsequently, approximately 30 ps of constant pressure and temper-

ature simulation (NPT) was carried out to equilibrate the system, which was followed by 30 ps of production simulation performed under the same conditions, using periodic boundary conditions with constant pressure, and the Berendsen barostat for constant pressure simulation. The temperature was controlled via Langevin dynamics (Boys and Bernardi, 1970) with collision frequency of 1 ps^{-1} . A cutoff of 16 \AA was used for nonbonded interactions and long-range electrostatic interactions were treated by means of the Particle Mesh Ewald (PME) method (Rassolov et al., 1998). All bonds involving hydrogen were constrained by the SHAKE method (Ryckaert et al., 1977) and the time step for numerical integration was 2 fs. The simulation results were analyzed using the cpptraj program in the Ambertools19 package (Roe and Cheatham, 2013). The diagram of density, energies, temperature and RMSD obtained by MD study of the 3FC2 protein along with molecules 1, 2 and 4 are displayed in Figs. 8-10.

The noteworthy points with the energy plot are that all of the energy terms increased during the first 20 ps, corresponding to heating from 0 K to 300 K. Then all energies are leveled off and remained constant for the remainder of the simulation indicating that the relaxation was completed and that an equilibrium has been reached. The system behaves in an expected

manner, the temperature started at 0 K and then increased to 300 K over a period of about 20 ps. The temperature then remained constant for the remainder of the simulation which means that the use of Langevin dynamics for temperature regulation is successful. The system has equilibrated at a density of approximately 1.02 g cm^{-3} , as the density of pure liquid water at 300 K is approximately 1.00 g cm^{-3} , this seems to be reasonable so adding the 3FC2 protein has increased the density by around 2 %. The RMSD increases very fast in the first 20 ps. There is not any significant conformational change in dihedral angles in the protein. RMSD values less than $1.5\text{-}0.2.0 \text{ \AA}$ are indicating a stable structure. The structures obtained at the end of MD production are represented in Fig. 11.

5. Biological activities section

5.1. Cytotoxic activity

One way to treat cancer is to use strong chemical drugs or chemotherapy. Today, several chemical drugs have been used and researched to treat cancer. It is important to find new drugs that can fight cancer cells.

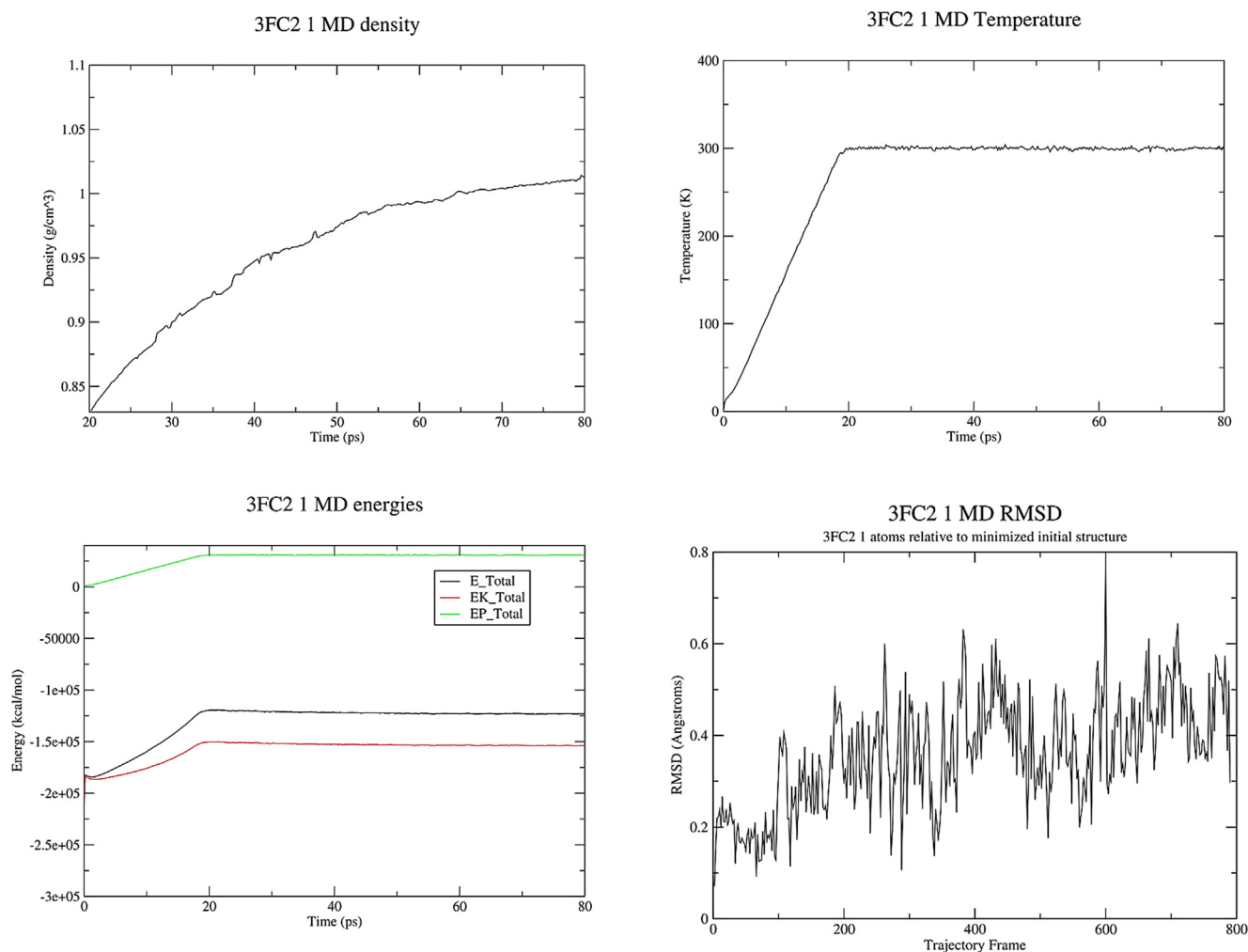


Fig. 8 Properties of the system 3FC2 protein and ligand 1 during the MD production.

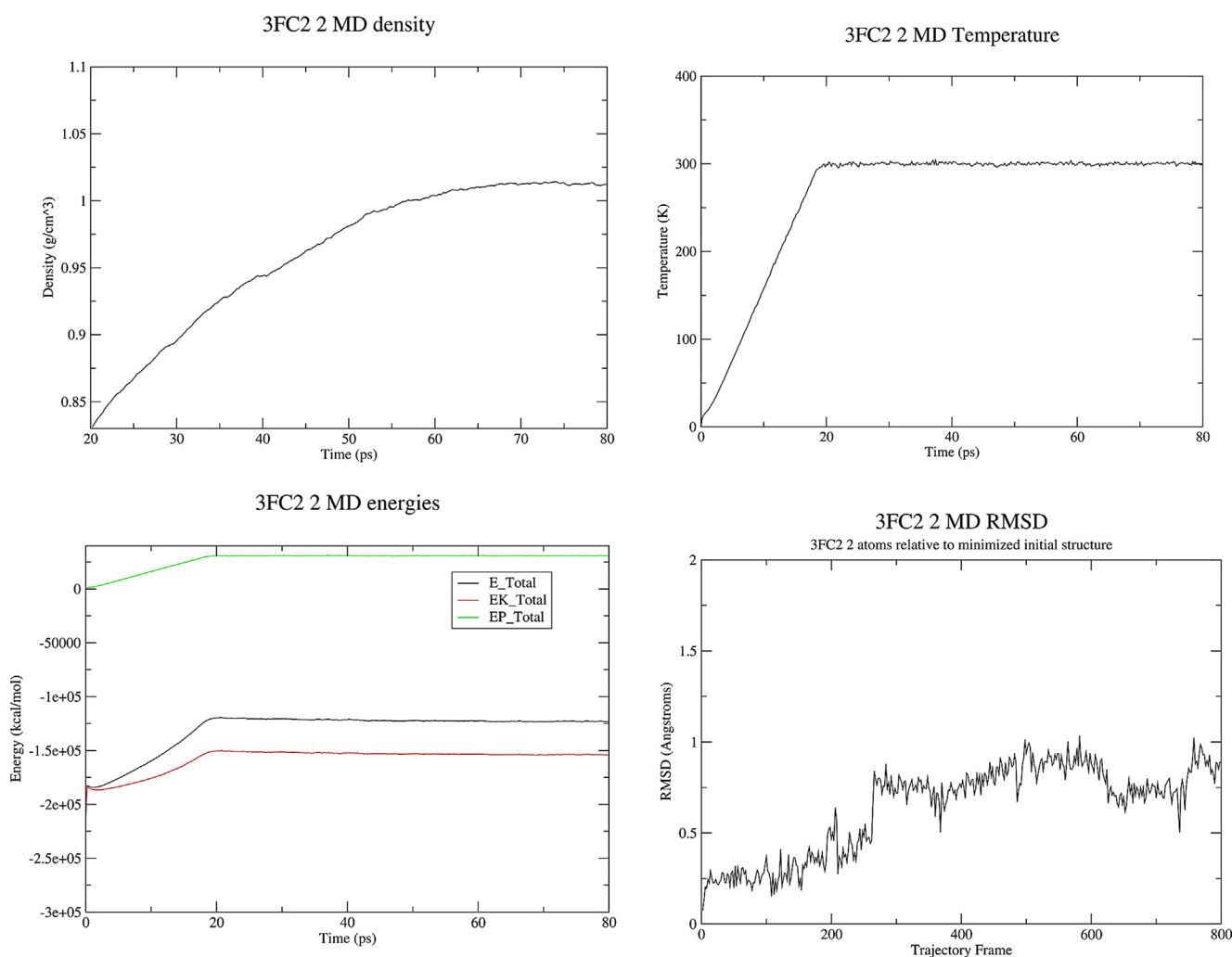


Fig. 9 Properties of the system 3FC2 protein and ligand 2 during the MD production.

Cell lines: We obtained breast cancer cells (MCF-7) from the Pasteur Institute of Iran (Tehran, Iran). The cells were stored at 37 °C in a humid atmosphere (90 %) containing 5 % CO₂ and then in DMEM (Dulbecco modified Eagle medium) with 10 % (v/v) FBS (bovine fetal serum), 100 units per ml different concentrations of samples 1–6 and vinblastine (Vin) were incubated with seed cells overnight.

Cell viability assay: The MTT reduction method has been used to estimate cell viability after exposure to synthetic compounds (Abd Alhameed et al., 2019; Yazdani Nyaki et al., 2021). Cells (MCF-7) were implanted in 96-well plates per 10,000 cells in each well containing a 200 µl medium. After 24 hr. of incubation at 37 °C, different concentrations of test compounds were added to the wells. Samples were tested 1–6 with Vin at the following concentrations: 20, 40, 60, 80, and 100 µg / mL. The samples were dissolved in dimethyl sulfoxide (DMSO) and then diluted with a cell culture medium, and after cell destruction, formazan dye was formed, indicating the mitochondria of living cells. In all treatments, including blank, the final concentration of DMSO was 1 % of the total volume of the medium. Cell viability was then calculated by MTT as a percentage of control (untreated cells) Fig. 12.

The anti-cancer activity of azo-sulfonamides designed in vitro against MCF-7 cells was tested by MTT assay and

Vin was used as the reference drug. The tested compounds were used in different concentrations and cell survival was determined after incubation for 24 h. Inhibition of cell proliferation in each treatment is reported as a percentage of the number of cells treated with untreated control cells Fig. 12. Cytotoxic activity in new derivatives is shown as IC₅₀ (µM) values Fig. 13.

In the designed azo-sulfonamide series, various aliphatic and aromatic alternatives showed promising cytotoxicity, with some compounds showing significant IC₅₀ values of the reference compound, Vin.

Fig. 13 shows IC₅₀ values 1-6. As a positive control, Vin with an IC₅₀ of approximately 11.46 µM was the same under all conditions. As can be seen in Fig. 13, the results of the MTT Assay test show that sample 5 has a stronger toxin property than other compounds. However, all IC₅₀ values showed almost reasonable activity for the compounds. Among the tested compounds, derivatives 5, 4, and 6 showed proliferative activity with IC₅₀ of 32.28, 32.66, and 35.35 µM, respectively.

Based on the obtained results, it seems that compound 5 contains a benzene ring and salicylic aldehyde coupling group, as well as also in samples 4 and 6 the presence of thiazole, isoxazole, 2-naphthol, and salicylic aldehyde groups, shows more toxicity and activity in inhibiting MCF-7 cell human prolifer-

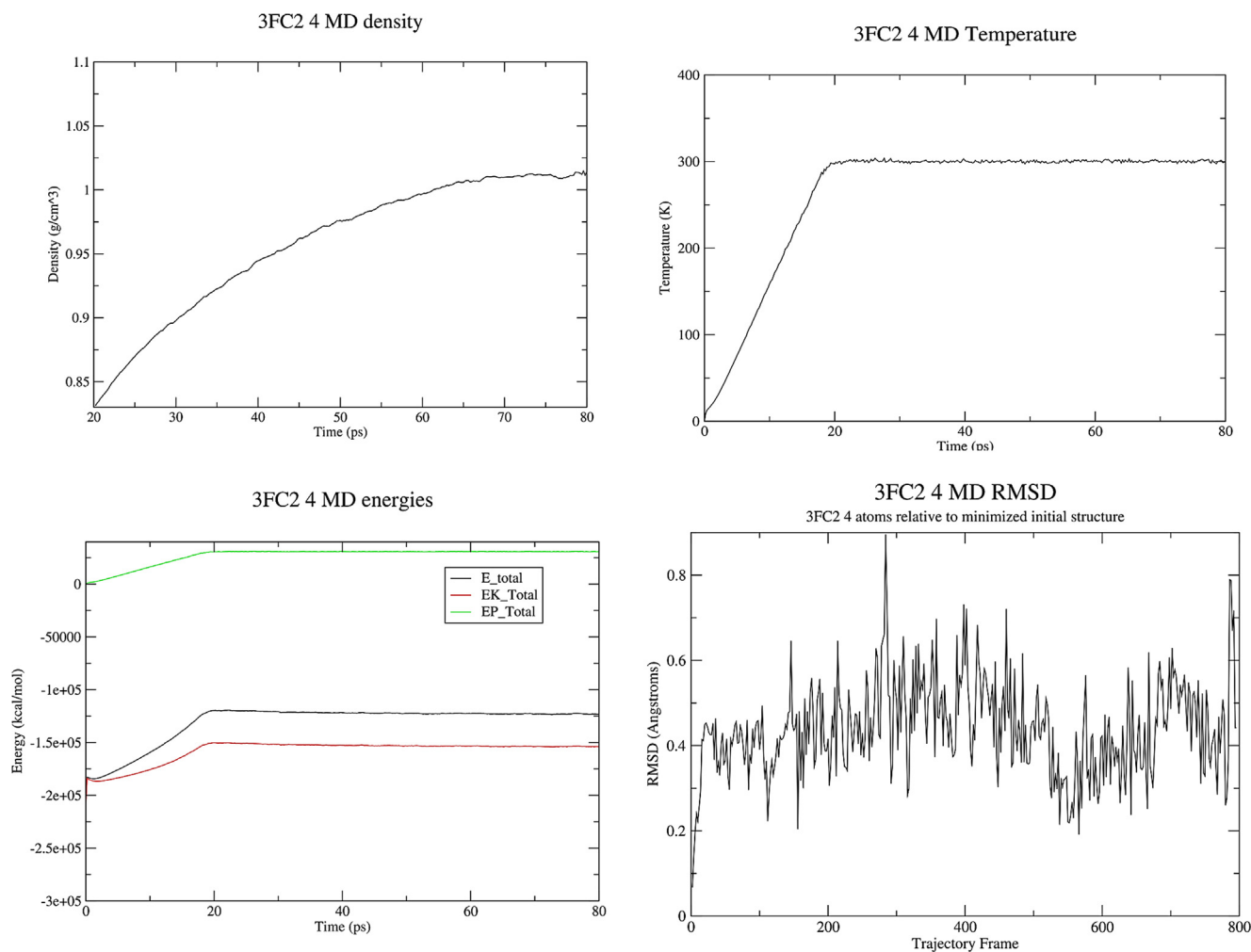


Fig. 10 Properties of the system 3FC2 protein and ligand 4 during the MD production.

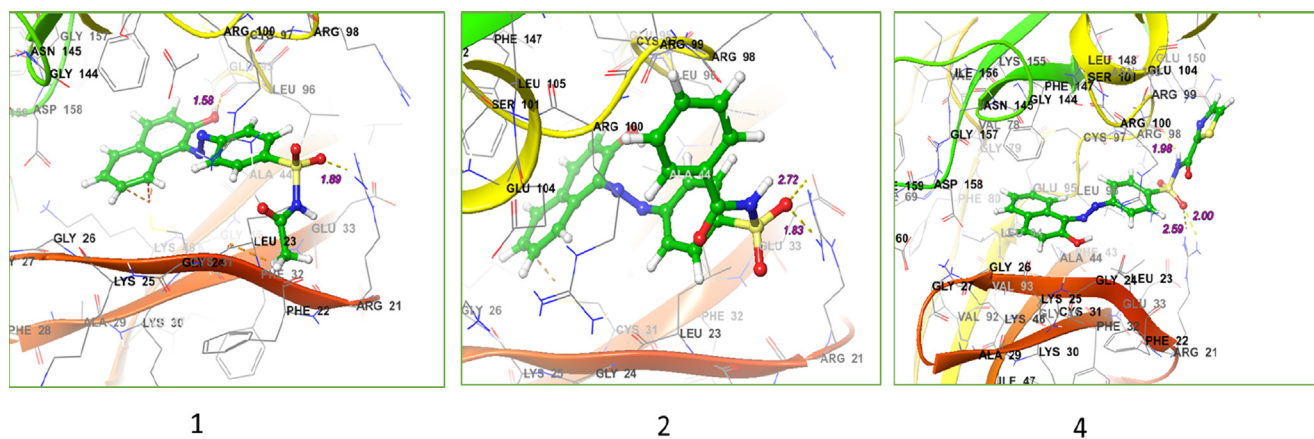


Fig. 11 Structure of the system after MD production for 3FC2 protein along with ligands 1, 2 and 4.

ation. Thus, these compounds are less effective against breast cells than positively controlled Vin. The MTT toxicity of compounds 1–6 compared to Vin is thus $5 > 4 > 6 > 2 > 3 > 1$ (Fig. 13).

In addition, the findings of the MTT experiment showed that the technique adopted between the sulfonamide and the mating group provided highly active compounds, making them very promising candidates for further research. The present

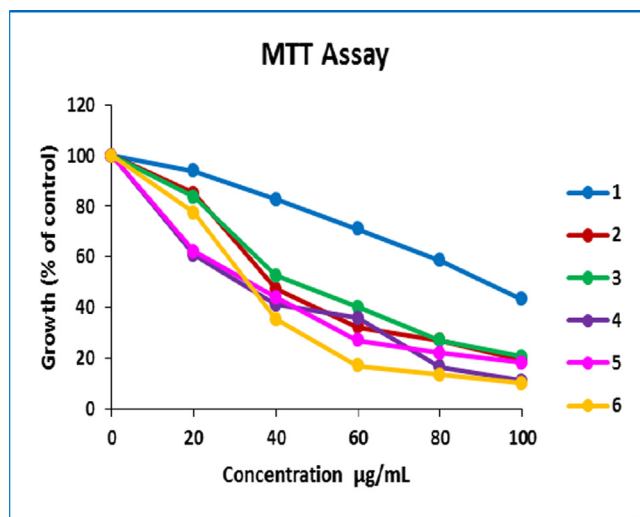


Fig. 12 MTT assay synthesized derivatives diagram.

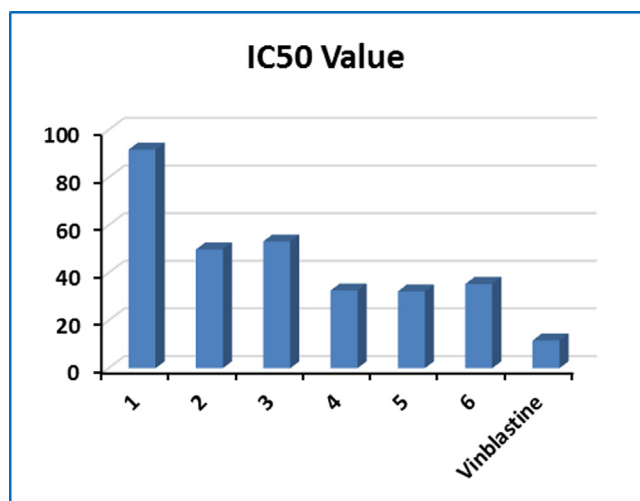


Fig. 13 Graph IC₅₀ values of synthesized derivatives.

study focused on investigating the potential anticancer mechanism of a new sulfasalazine analog compound in MCF-7 cells.

6. Experimental

6.1. Chemicals and devices

The chemicals and solvents used in this study were prepared by Merck & Aldridge companies as follows: cellulose, chlorine and sulfonic acid, MeOH, acetone, EtOAc, and NaNO₂, as well as sulfonamide derivatives from the drug company (Caspitantamin) prepared, this material was used without further purification. To follow the reaction process, thin layer chromatography (TLC) with aluminum plates and silica gel 60 F254 and ultraviolet lamps were used. The melting points of the synthesized compounds were measured with the melting point measuring device of Model 9100 Electrothermal and reported as uncorrected. IR spectra were recorded by JASCO

FT/IR-4700 infrared spectrometer. ¹H NMR and ¹³C NMR spectra were obtained with Bruker Avance 500 MHz using TMS as internal standard and in DMSO solvent at r. t.

6.2. Catalyst preparation

The cellulose-sulfuric acid was prepared according to the literature (Shaabani and Maleki, 2007). After completion of the reaction and separation of the organic compounds, cellulosic sulfuric acid (CSA) was recovered. For this purpose, the CSA was first washed with EtOH and MeOH, then placed at 70 °C for 24 h to dry completely. The recovered catalyst was used three more times for the above reaction, which could be performed without significant change in CSA activity.

6.3. Method for the synthesis of new azo-sulfonamide derivatives

At first, a homogeneous mixture was obtained by grinding sulfonamides (type 1 amine) (2 mmol) and cellulosic sulfuric acid (1.5 g) with a few drops of water (0.2 ml) in a mortar. NaNO₂ (4 mmol, 0.138 g) was then added to the resulting mixture and gently ground for 2–3 min. The presence of diazonium salt was confirmed by the beta naphthol. The reaction mixture was reacted with the coupling agent for 10–20 min. Reaction progress was tracked using TLC. After the reaction was complete, the mixture contained in acetone (10 ml) was dissolved and separated from sulfuric acid by filtration, then washed 3 more times with acetone (10 ml). The solution was evaporated under filtration and the remaining solids were crystallized with EtOH and H₂O. The newly obtained azo-sulfonamide derivatives with good yield (60–93 %) and a short reaction time 20–35 min. In Table 1, the general results of azo-sulfonamide derivatives with various substitutions are reported. Fig. 2 and Table 1.

Physical properties and spectral data for synthesized products.

(E)-N-((4-((2-hydroxynaphthalen-1-yl)diazenyl)phenyl)sulfonyl)acetamide (**1**).

Orange powder, efficiency: 81 %, m.p: 287 °C; FT-IR (KBr, ν/cm^{-1}): 3428 (O–H stretch), 2859 (aliphatic C–H stretch), 1723 (C=O stretch), 1592 (aromatic C=C stretch), 1438 (N=N stretch), 1254 (C–O stretch), 1337, 1147 (symmetric SO₂ stretch), 856 + 660 (aromatic C–H out-of-plane bend). ¹H NMR (400 MHz, DMSO *d*₆) δ : 1.98 (t, *J* = 4.2, 2.2 Hz, 3H), 6.80 (d, *J* = 9.6 Hz, 1H), 7.52–7.55 (t, *J* = 6.2, 2.0 Hz, 1H), 7.64–7.67 (t, *J* = 4.0, 1.2 Hz, 1H), 7.84 (d, *J* = 7.56 Hz, 1H), 8.49 (d, *J* = 7.28 Hz, 1H), 7.98–8.04 (m, 5H), 12.17 (s, 1H), 15.80 (s, 1H). ¹³C NMR (100 MHz, DMSO *d*₆) δ : 178, 169.43, 147.24, 143.39, 36.15, 133.13, 131.02, 130.15, 129.97, 129.79, 128.71, 127.69, 126.31, 122.46, 17.77, and 23.82. HRMS-ESI (*m/z*) [*M*⁺] Calcd. for C₁₈H₁₅N₃O₄S 369.0825, found 369.0911. Elemental Analysis Calcd. for C₁₈H₁₅N₃O₄S (%): C, 58.53; H, 4.09; N, 11.38; O, 17.32; S, 8.68 Found: C, 59.13; H, 4.33; N, 10.68; O, 18.65; S, 7.21.

(E)-N-((4-((2-hydroxynaphthalen-1-yl)diazenyl)phenyl)sulfonyl)benzamide (**2**).

Orange powder, efficiency: 83 %, m.p: 291 °C; FT-IR (KBr, ν/cm^{-1}): 2982 (aliphatic C–H stretch), 1447 (N=N stretch), 1232 (C–O stretch), 1146 (symmetric SO₂ stretch). ¹H NMR (400 MHz, DMSO *d*₆) δ : 6.8 (d, *J* = 9.4 Hz, 1H), 7.28–7.35 (m, 2H), 7.36–7.38 (m, 1H), 7.45–7.49 (m, 1H), 7.60–7.64 (m,

1H), 7.7 (d, $J = 7.6$ Hz, 1H), 7.8 (d, $J = 8.1$ Hz, 2H), 7.89–7.92 (m, 2H), 8.53 (d, $J = 8.1$ Hz, 1H), 7.94–7.97 (m, 3H). ^{13}C NMR (100 MHz, *DMSO* d_6) δ : 172.35, 170.20, 145.52, 145.40, 141.42, 139.70, 133.22, 130.32, 130.10, 129.79, 129.49, 129.11, 128.78, 128.38, 127.84, 126.72, 125.12, 122.00, and 117.90. HRMS-ESI (*m/z*) [M^+] Calcd. for $\text{C}_{23}\text{H}_{17}\text{N}_3\text{O}_4\text{S}$ 431.0945, found 431.1138. Elemental Analysis Calcd. for $\text{C}_{23}\text{H}_{17}\text{N}_3\text{O}_4\text{S}$ (%): C, 64.03; H, 3.97; N, 9.74; O, 14.83; S, 7.43 Found: C, 63.88; H, 4.11; N, 9.56; O, 15.03; S, 7.42.

(E)-N-((4-(2-hydroxynaphthalen-1-yl)diazenyl)phenyl)sulfonyl)-5-methylisoxazole-3-carboxamide (**3**).

Orange powder, efficiency: 64 %, m.p: 207 °C; FT-IR (KBr, ν/cm^{-1}): 3071 (aromatic C—H stretch), 2859 (aliphatic C—H stretch), 1614 (N—H stretch in R2-NH), 1593 (aromatic C=C stretch), 1466 (N=N stretch), 1149 (asymmetric SO_2 stretch), 1255 (C—O stretch) 1149 (symmetric SO_2 stretch). ^1H NMR (400 MHz, *DMSO* d_6) δ : 2.38 (s, 3H), 6.79 (d, $J = 9.06$ Hz, 1H), 6.08 (s, 1H), 7.47–7.51 (t, $J = 6.2$, 3.1 Hz, 2H), 7.59–7.63 (t, $J = 4.5$, 2.1 Hz, 1H), 8.47 (d, $J = 8.0$ Hz, 1H), 7.88–7.97 (m, 5H), 11.49 (s, 1H), 15.76 (s, 1H). ^{13}C NMR (100 MHz, *DMSO* d_6) δ : 177.56, 170.60, 158.47, 147, 143.25, 136.72, 136.35, 133.11, 130.94, 130.12, 129.76, 129.08, 128.68, 127.62, 126.22, 122.45, 118.14, 96.01, and 12.55. HRMS-ESI (*m/z*) [M^+] Calcd. for $\text{C}_{21}\text{H}_{16}\text{N}_4\text{O}_5\text{S}$ 436.4474, found 436.6521. Elemental Analysis Calcd. for $\text{C}_{21}\text{H}_{16}\text{N}_4\text{O}_5\text{S}$ (%): C, 57.79; H, 3.70; N, 12.84; O, 18.33; S, 7.35 found: C, 56.88; H, 4.15; N, 13.25; O, 17.04; S, 8.68.

(E)-N-((4-(2-hydroxynaphthalen-1-yl)diazenyl)phenyl)sulfonyl)thiazole-2-carboxamide (**4**).

Orange powder, efficiency: 74 %, m.p: 205 °C; FT-IR (KBr, ν/cm^{-1}): 3209 (O—H stretch), 1722 (C=O stretch), 1590 (aromatic C=C stretch), 1434 (N=N stretch), 1363 (asymmetric SO_2 stretch), 1140 (symmetric SO_2 stretch). ^1H NMR (400 MHz, *DMSO* d_6) δ : 15.81 (s, 1H), 12.86 (s, 1H), 8.47 (d, $J = 8.0$, 1H), 7.96 (d, $J = 9.6$ Hz, 1H), 7.88–7.93 (m, 4H), 7.76 (d, $J = 7.4$ Hz, 1H), 7.59–7.63 (m, 1H), 7.46–7.50 (m, 1H), 7.25 (d, $J = 4.52$ Hz, 1H), 6.80–6.83 (t, $J = 8.2$, 4.2 Hz, 2H). ^{13}C NMR (100 MHz, *DMSO* d_6) δ : 175.7, 169.3, 146.3, 142.6, 140.3, 133.1, 130.5, 130.0, 129.6, 128.5, 128.08, 127.02, 108.7, 118.2, 122.02, 125.7, and 126.2. HRMS-ESI (*m/z*) [M^+] Calcd. for $\text{C}_{20}\text{H}_{14}\text{N}_4\text{O}_4\text{S}_2$ 438.0572, found 438.1065. Elemental Analysis Calcd. for $\text{C}_{20}\text{H}_{14}\text{N}_4\text{O}_4\text{S}_2$ (%): C, 54.79; H, 3.22; N, 12.78; O, 14.60; S, 14.62 found: C, 55.02; H, 4.26; N, 12.55; O, 13.28; S, 14.89.

(E)-N-((4-(3-formyl-4-hydroxyphenyl)diazenyl)phenyl)sulfonyl)benzamide (**5**).

Orange powder, efficiency: 87 %, m.p: 225 °C; FT-IR (KBr, ν/cm^{-1}): 3605 (O—H stretch), 3059 (aromatic C—H stretch), 1692 (aldehyde C=O stretch), 1582 (aromatic C=C stretch), 1477 (N=N stretch), 1344 (asymmetric SO_2 stretch), 1265 (C—O stretch). ^1H NMR (400 MHz, *DMSO* d_6) δ : 10.32 (s, 1H), 8.13 (d, $J = 2.7$ Hz, 1H), 8.02 (dd, $J = 9.0$, 2.7 Hz, 1H), 7.93 (d, $J = 8.6$ Hz, 2H), 7.84 (d, $J = 8.6$ Hz, 2H), 6.97 (d, $J = 9.0$ Hz, 1H), 1.76 (s, 3H). ^{13}C NMR (100 MHz, *DMSO* d_6) δ : 190.82, 166.76, 164.51, 154.56, 145.28, 142.41, 133.28, 130.41, 129.54, 128.91, 124.90, 123.21, 123.04, and 119.06. HRMS-ESI (*m/z*) [M^+] Calcd. For $\text{C}_{20}\text{H}_{15}\text{N}_3\text{O}_5\text{S}$ 409.0741, found 409.1158. Elemental Analysis Calcd. For $\text{C}_{20}\text{H}_{15}\text{N}_3\text{O}_5\text{S}$ (%): C, 58.67; H, 3.69; N, 10.26; O, 19.54; S, 7.83 Found: C, 57.99; H, 3.75; N, 11.32; O, 19.20; S, 7.74.

(E)-N-((4-(3-formyl-4-hydroxyphenyl)diazenyl)phenyl)sulfonyl)-5-methylisoxazole-3-carboxamide (**6**).

Orange powder, efficiency: 79 %, m.p: 213 °C; FT-IR (KBr, ν/cm^{-1}): 3794 (O—H stretch), 1727 1659 ν (C=O stretch), 1581 (aromatic C=C stretch), 1479 (N=N stretch), 1349, 1137 (symmetric SO_2 stretch), 1283 (C—O stretch). ^1H NMR (400 MHz, *DMSO* d_6) δ : 10.37 (s, 1H), 8.2 (d, $J = 5.1$ Hz, 1H), 8.11–8.14 (dd, $J = 7.5$, 3.4 Hz, 1H), 8.01–8.06 (d, $J = 8.1$ Hz, 4H), 7.2 (dd, $J = 8.88$, 3.8 Hz, 1H), 2.51–2.52 (t, $J = 7.4$, 4.1 Hz, 3H), 6.18 (s, 1H). ^{13}C NMR (100 MHz, *DMSO* d_6) δ : 190.80, 170.97, 164.67, 154.69, 145.20, 141.16, 130.40, 128.72, 124.97, 123.49, 123.21, 119.08, 95.96, and 12.56. HRMS-ESI (*m/z*) [M^+] Calcd. for $\text{C}_{18}\text{H}_{14}\text{N}_4\text{O}_6\text{S}$ 414.0623, found 414.0847. Elemental Analysis Calcd. for $\text{C}_{18}\text{H}_{14}\text{N}_4\text{O}_6\text{S}$ (%): C, 52.17; H, 3.41; N, 13.52; O, 23.17; S, 7.74 Found: C, 52.25; H, 4.68; N, 13.11; O, 22.84; S, 7.12.

7. Conclusion

Here several new azo-sulfonamide compounds as sulfasalazine pseudo-analog derivatives with decent performance and good yield and the ability to form hydrogen bonds with the active sites of the receptor were synthesized. Further, the biological properties of synthesis compounds were investigated by MTT assay and molecular docking, the synthesized products showed reasonable biological properties. To check the efficiency of the synthesized molecules as anticancer drugs, docking simulation was performed in the active sites of three target cell line proteins (MCF-7) using the Schrodinger program package. The results show that there are effective interactions between the ligand and the receptor. In examining the cytotoxicity of the products on the human breast cell line, it was found that all compounds have anticancer activity, and the IC_{50} values showed almost reasonable activity for all compounds. The synthesized derivatives showed good biological results and can be a basis for further research in this field. The properties obtained by the MD simulation of the 3FC2 protein and the three highest scores ligand (1, 2, and 4) in the docking study which involves energy, density temperature, and RMSD values altogether lead to the conclusion that the system has reached to a stable structure.

Declaration of Competing Interest

The authors declare that they have no known competing financial interests or personal relationships that could have appeared to influence the work reported in this paper.

Acknowledgments

This probe was supported in part by the Research Committee of the University of Guilan.

Appendix A. Supplementary material

Supplementary data to this article can be found online at <https://doi.org/10.1016/j.arabjc.2022.104383>.

References

- Abd Alhameed, R., Almarhoon, Z., Bukhari, S.I., El-Faham, A., de la Torre, B.G., Albericio, F., 2019. Synthesis and antimicrobial activity of a new series of thiazolidine-2, 4-diones carboxamide and amino acid derivatives. *Molecules* 25, 105.
- Agre, A.M., Upade, A.C., Yadav, M.A., Kumbhar, S.B., 2021. A Review on Breast Cancer and its Management.
- Ali, Y., Hamid, S.A., Rashid, U., 2018. Biomedical applications of aromatic azo compounds. *Mini Rev. Med. Chem.* 18, 1548–1558.

- Ansari, M.J., Aldawsari, M.F., Zafar, A., Soltani, A., Yasir, M., Jahangir, M.A., Taleuzzaman, M., Erfani-Moghadam, V., Daneshmandi, L., Mahmoodi, N.O., 2022. In vitro release and cytotoxicity study of encapsulated sulfasalazine within LTSP micellar/liposomal and TSP micellar/niosomal nano-formulations. *Alexandria Eng. J.* 61, 9749–9756.
- Bakadia, B.M., Manan, S., Ul-Islam, M., Mukole, B.M., Shahzad, A., Abdalla, A.M.E., Ullah, M.W., Yang, G., 2022. Microbiome as Cancer Biomarkers. In: *Cancer Biomarkers in Diagnosis and Therapeutics*. Springer, pp. 101–148.
- Becke, A.D., 1993. Density-functional thermochemistry. III. The role of exact exchange. *J. Chem. Phys.* 98, 5648–5652. <https://doi.org/10.1063/1.464913>.
- Binning, R.C., Curtiss, L.A., 1990. Compact contracted basis sets for third-row atoms: Ga–Kr. *J. Comput. Chem.* 11, 1206–1216. <https://doi.org/10.1002/jcc.540111013>.
- Blaudeau, J.P., McGrath, M.P., Curtiss, L.A., Radom, L., 1997. Extension of Gaussian-2 (G2) theory to molecules containing third-row atoms K and Ca. *J. Chem. Phys.* 107, 5016–5021. <https://doi.org/10.1063/1.474865>.
- Boys, S.F., Bernardi, F., 1970. The calculation of small molecular interactions by the differences of separate total energies. Some procedures with reduced errors. *Mol. Phys.* 19, 553–566. <https://doi.org/10.1080/00268977000101561>.
- Burden, G., Fitzmaurice, C., Akinyemiju, T.F., Al Lami, F.H., Alam, T., Alizadeh-Navaei, R., Allen, C., Alsharif, U., Alvis-Guzman, N., Amini, E., 2018. Global, regional, and national cancer incidence, mortality, years of life lost, years lived with disability, and disability-adjusted life-years for 29 cancer groups, 1990 to 2016: a systematic analysis for the global burden of disease study. *JAMA Oncol.* 4, 1553–1568.
- Camarillo, I., Thulasidas, J.S., Poopavai, S., 2021. Male Breast Cancer: Another Look.
- Chauhan, A., Kaith, B., 2011. X-Ray Diffraction studies and assessment of Roselle graft-copolymers. *Malaysian Polym. J.* 6, 155–164.
- Chauhan, A., Kaith, B., 2012. X-Ray Powder Diffraction Studies to Evaluate the Transition in Graft Copolymers Procured from Roselle Fiber. *J. Nat. Fibers* 9, 87–97.
- Choudhary, M., Kumar, V., Malhotra, H., Singh, S., 2015. Medicinal plants with potential anti-arthritis activity. *J. Intercult. Ethnopharmacol.* 4, 147.
- Cockerham, C., Caruthers, A., McCloud, J., Fortner, L.M., Youn, S., McBride, S.P., 2022. Azo-Dye-Functionalized Polycarbonate Membranes for Textile Dye and Nitrate Ion Removal. *Micromachines* 13, 577.
- Crespi, S., Simeth, N.A., König, B., 2019. Heteroaryl azo dyes as molecular photoswitches. *Nat. Rev. Chem.* 3, 133–146.
- Cullity, B.D., 1978. Diffraction under nonideal conditions. *Elem. X-ray Diffr.*, 107–145.
- David, T.I., Adelakun, N.S., Omotuyi, O.I., Metibemu, D.S., Ekun, O. E., Inyang, O.K., Adewumi, B., Enejoh, O.A., Owolabi, R.T., Oribamise, E.I., 2018. Molecular docking analysis of phyto-constituents from Cannabis sativa with pFDHFR. *Bioinformation* 14, 574.
- Ditchfield, R., Hehre, W.J., Pople, J.A., 1971. Self-consistent molecular-orbital methods. IX. An extended gaussian-type basis for molecular-orbital studies of organic molecules. *J. Chem. Phys.* 54, 720–723. <https://doi.org/10.1063/1.1674902>.
- Elsellami, L., 2008. Élimination d'acides aminés par complexation avec des composés calixaréniques et par dégradation photocatalytique.
- Francl, M.M., Pietro, W.J., Hehre, W.J., Binkley, J.S., Gordon, M.S., DeFrees, D.J., Pople, J.A., 1982. Self-consistent molecular orbital methods. XXIII. A polarization-type basis set for second-row elements. *J. Chem. Phys.* 77, 3654–3665. <https://doi.org/10.1063/1.444267>.
- Frisch, M.J., Trucks, G., Schlegel, H.B. e al, Scuseria, G.E. w, Robb, M.A., Cheeseman, J.R., Montgomery Jr, J.A., Vreven, T., Kudin, K.N., Burant, J.C., 2004. Gaussian 03, revision C. 02.
- Gaffer, H.E., 2019. Antimicrobial sulphonamide azo dyes. *Color. Technol.* 135, 484–500.
- Gaffer, H.E., Elgohary, M.R., Etman, H.A., Shaaban, S., 2017. Antibacterial evaluation of cotton fabrics by using novel sulfonamide reactive dyes. *Pigment Resin Technol.*
- Ganewatta, M.S., Lokupitiya, H.N., Tang, C., 2019. Lignin biopolymers in the age of controlled polymerization. *Polymers (Basel)*. 11. <https://doi.org/10.3390/polym11071176>.
- Ganjali, M.R., Faridbod, F., Dinarvand, R., Norouzi, P., Riahi, S., 2008. Schiff's bases and crown ethers as supramolecular sensing materials in the construction of potentiometric membrane sensors. *Sensors* 8, 1645–1703. <https://doi.org/10.3390/s8031645>.
- Gilani, A.G., Yazdanbakhsh, M.R., Mahmoodi, N., Moghadam, M., Moradi, E., 2008. Solvatochromism and dichroism of fluorinated azoquinolin-8-ol dyes in liquid and liquid crystalline solutions. *J. Mol. Liq.* 139, 72–79.
- Gomberg, M., Bachmann, W.E., 1924. The synthesis of biaryl compounds by means of the diazo reaction. *J. Am. Chem. Soc.* 46, 2339–2343.
- Gordon, P.F., Gregory, P., 2022. Organic chemistry in colour. *Organic Chemistry in Colour*. De Gruyter.
- Hari, D.P., Koenig, B., 2013. The photocatalyzed meerwein arylation: classic reaction of aryl diazonium salts in a new light. *Angew. Chemie Int. Ed.* 52, 4734–4743.
- Hariharan, P.C., Pople, J.A., 1973. The influence of polarization functions on molecular orbital hydrogenation energies. *Theor. Chim. Acta* 28, 213–222. <https://doi.org/10.1007/BF00533485>.
- Hariharan, P.C., Pople, J.A., 1974. Accuracy of AHn equilibrium geometries by single determinant molecular orbital theory. *Mol. Phys.* 27, 209–214. <https://doi.org/10.1080/00268977400100171>.
- Hehre, W.J., Ditchfield, K., Pople, J.A., 1972. Self-consistent molecular orbital methods. XII. Further extensions of gaussian-type basis sets for use in molecular orbital studies of organic molecules. *J. Chem. Phys.* 56, 2257–2261. <https://doi.org/10.1063/1.1677527>.
- Kenchegowda, M., Rahamathulla, M., Hani, U., Begum, M.Y., Guruswamy, S., Osmani, R.A.M., Gowrav, M.P., Alshehri, S., Ghoneim, M.M., Alshlowi, A., 2022. Smart Nanocarriers as an Emerging Platform for Cancer Therapy: A Review. *Molecules* 27, 146.
- Keshavayya, J., 2019. Synthesis, structural investigations and in vitro biological evaluation of N, N-dimethyl aniline derivatives based azo dyes as potential pharmacological agents. *J. Mol. Struct.* 1186, 404–412.
- Khan, M.N., Parmar, D.K., Das, D., 2021. Recent Applications of Azo Dyes: A Paradigm Shift from Medicinal Chemistry to Biomedical Sciences. *Mini Rev. Med. Chem.* 21, 1071–1084.
- Krishnan, R., Binkley, J.S., Seeger, R., Pople, J.A., 1980. Self-consistent molecular orbital methods. XX. A basis set for correlated wave functions. *J. Chem. Phys.* 72, 650–654. <https://doi.org/10.1063/1.438955>.
- Kumar, G., Kumar, D., Singh, C.P., Kumar, A., Rana, V.B., 2010. Synthesis, physical characterization and antimicrobial activity of trivalent metal Schiff base complexes. *J. Serbian Chem. Soc.* 75, 629–637.
- Lee, C., Yang, W., Parr, R.G., 1988. Development of the Colle-Salvetti correlation-energy formula into a functional of the electron density. *Phys. Rev. B* 37, 785–789. <https://doi.org/10.1103/PhysRevB.37.785>.
- Lina, L., 2021. Signs and Symptoms of Breast cancer. *Eur. J. Clin. Oncol.* 3, 1.
- Mahmoodi, N.O., Pasandideh Nadamani, M., Behzadi, T., 2013. New 1,3-diazabicyclo-[3.1.0]hex-3-ene photochromic azo dyes: Synthesis, characterization and spectroscopic studies. *J. Mol. Liq.* 187, 43–48. <https://doi.org/10.1016/j.molliq.2013.05.026>.

- Mahmoodi, N.O., Rahimi, S., Pasandideh Nadamani, M., 2017. Microwave-assisted synthesis and photochromic properties of new azo-imidazoles. *Dye. Pigment.* 143, 387–392. <https://doi.org/10.1016/j.dyepig.2017.04.053>.
- Malaekhepoor, S.M., Derakhshandeh, K., Haddadi, R., Nourian, A., Ghorbani-Vaghei, R., 2020. A polymer coated MNP scaffold for targeted drug delivery and improvement of rheumatoid arthritis. *Polym. Chem.* 11, 2408–2417.
- Mane, P.T., Patil, S.P., Wakure, B.S., Wakte, P.S., 2021. Breast cancer: understanding etiology, addressing molecular signaling pathways, identifying therapeutic targets and strategizing the treatment. *Int. J. Res. Pharm. Sci.* 12, 1757–1769.
- McLean, A.D., Chandler, G.S., 1980. Contracted Gaussian basis sets for molecular calculations. I. Second row atoms, $Z=11-18$. *J. Chem. Phys.* 72, 5639–5648. <https://doi.org/10.1063/1.438980>.
- Mote, V.D., Purushotham, Y., Dole, B.N., 2012. Williamson-Hall analysis in estimation of lattice strain in nanometer-sized ZnO particles. *J. Theor. Appl. Phys.* 6, 1–8.
- Nadamani, M.P., Mahmoodi, N.O., Mamaghani, M., Zanjanchi, M. A., Nahzomi, H.T., 2019. Photochromic Properties of Novel One-pot Multicomponent Synthesized Tetraarylimidazoles. *ChemistrySelect* 4, 8470–8476.
- Nemati, F., Elhampour, A., 2012. Cellulose sulphuric acid as a biodegradable catalyst for conversion of aryl amines into azides at room temperature under mild conditions. *J. Chem. Sci.* 124, 889–892. <https://doi.org/10.1007/s12039-012-0261-1>.
- Nyaki, H.Y., Mahmoodi, N.O., 2021. Synthesis and characterization of derivatives including thiazolidine-2, 4-dione/1-H-imidazole and evaluation of antimicrobial, antioxidant, and cytotoxic properties of new synthetic heterocyclic compounds. *Res. Chem. Intermed.* 47, 4129–4155.
- Parekh, S.P., 2010. Synthesis and characterization of pharmacologically active compounds.
- Pervaiz, M., Sadiq, S., Sadiq, A., Younas, U., Ashraf, A., Saeed, Z., Zuber, M., Adnan, A., 2021. Azo-Schiff base derivatives of transition metal complexes as antimicrobial agents. *Coord. Chem. Rev.* 447, 214128.
- Peters, A.T., Freeman, H.S., 1991. *Colour chemistry: the design and synthesis of organic dyes and pigments*. Springer.
- Rassolov, V.A., Pople, J.A., Ratner, M.A., Windus, T.L., 1998. 6–31G* basis set for atoms K through Zn. *J. Chem. Phys.* 109, 1223–1229. <https://doi.org/10.1063/1.476673>.
- Ravi, B.N., Keshavayya, J., Kumar, V., Kandgal, S., 2020. Synthesis, characterization and pharmacological evaluation of 2-aminothiazole incorporated azo dyes. *J. Mol. Struct.* 1204, 127493.
- Roe, D.R., Cheatham, T.E., 2013. PTRAJ and CPPTRAJ: Software for processing and analysis of molecular dynamics trajectory data. *J. Chem. Theory Comput.* 9, 3084–3095. <https://doi.org/10.1021/ct400341p>.
- Ryckaert, J.P., Ciccotti, G., Berendsen, H.J.C., 1977. Numerical integration of the cartesian equations of motion of a system with constraints: molecular dynamics of n-alkanes. *J. Comput. Phys.* 23, 327–341. [https://doi.org/10.1016/0021-9991\(77\)90098-5](https://doi.org/10.1016/0021-9991(77)90098-5).
- Shaabani, A., Maleki, A., 2007. Cellulose sulfuric acid as a bio-supported and recyclable solid acid catalyst for the one-pot three-component synthesis of α -amino nitriles. *Appl. Catal. A: General* 331, 149–151. <https://doi.org/10.1016/j.apcata.2007.07.021>.
- Shaikh, K., Krishnan, S., Thanki, R., 2021. Types, diagnosis, and treatment of breast cancer. In: *Artificial Intelligence in Breast Cancer Early Detection and Diagnosis*. Springer, pp. 21–35.
- Sharma, G.N., Dave, R., Sanadya, J., Sharma, P., Sharma, K., 2010. Various types and management of breast cancer: an overview. *J. Adv. Pharm. Technol. Res.* 1, 109.
- Sharma, R., Garg, R., Kumari, A., 2020. A review on biogenic synthesis, applications and toxicity aspects of zinc oxide nanoparticles. *EXCLI J.* 19, 1325.
- Sheykhi-Estakhjani, A., Mahmoodi, N.O., Yahyazadeh, A., Pasandideh Nadamani, M., 2020. Synthesis and antibacterial evaluation of diaminomaleonitrile-based azo-Schiff bases and 8,9-dihydro-7H-purine-6-carboxamides. *Res. Chem. Intermed.* 46, 3835–3852. <https://doi.org/10.1007/s11164-020-04175-y>.
- Smith, R.D., Mallath, M.K., 2019. History of the growing burden of cancer in India: from antiquity to the 21st century. *J. Glob. Oncol.* 5, 1–15.
- Song, L.F., Lee, T.S., Zhu, C., York, D.M., Merz, K.M., 2019. Using AMBER18 for Relative Free Energy Calculations. *J. Chem. Inf. Model.* 59, 3128–3135. <https://doi.org/10.1021/acs.jcim.9b00105>.
- Stephens, P.J., Devlin, F.J., Chabalowski, C.F., Frisch, M.J., 1994. Ab Initio calculation of vibrational absorption and circular dichroism spectra using density functional force fields. *J. Phys. Chem.* 98, 11623–11627. <https://doi.org/10.1021/j100096a001>.
- Sung, H., Ferlay, J., Siegel, R.L., Laversanne, M., Soerjomataram, I., Jemal, A., Bray, F., 2021. Global cancer statistics 2020: GLOBOCAN estimates of incidence and mortality worldwide for 36 cancers in 185 countries. *CA. Cancer J. Clin.* 71, 209–249.
- Vosko, S.H., Wilk, L., Nusair, M., 1980. Accurate spin-dependent electron liquid correlation energies for local spin density calculations: a critical analysis. *Can. J. Phys.* 58, 1200–1211. <https://doi.org/10.1139/p80-159>.
- Wang, J., Wolf, R.M., Caldwell, J.W., Kollman, P.A., Case, D.A., 2004. Development and testing of a general Amber force field. *J. Comput. Chem.* 25, 1157–1174. <https://doi.org/10.1002/jcc.20035>.
- Węglarz-Tomczak, E., Górecki, Ł., 2012. Barwniki azowe-aktywność biologiczna i strategie syntezy. *Chemik* 66.
- Wellings, S.R., Jensen, H.M., 1973. On the origin and progression of ductal carcinoma in the human breast. *J. Natl. Cancer Inst.* 50, 1111–1118.
- Yazdani Nyaki, H., Mahmoodi, N.O., Pasandideh Nadamani, M., 2021. Design and synthesis of a new tripod-chromogenic sensor based on a s-triazine and thiazolidine-2,4-dione ring (TCST) for naked-eye detection of Li^+ . *Can. J. Chem.* 99, 482–490. <https://doi.org/10.1139/cjc-2020-0366>.